Doppler Effect Mitigation using Reconfigurable Intelligent Surfaces with Hardware Impairments

Ke Wang, Chan-Tong Lam, and Benjamin K. Ng
School of Applied Sciences, Macao Polytechnic Institute
Macao S.A.R, China
Emails: {ke.wang; ctlam; bng}@ipm.edu.mo

2021 IEEE Globecom Workshops (GC Wkshps) | 978-1-6654-2390-8/21/$31.00 ©2021 IEEE | DOI: 10.1109/GCWkshps52748.2021.9681939

***Abstract*—In this paper, we analyze the effects of different types of hardware impairments (HWI), including RIS-HWI, transceiver HWI, phase quantization errors and random failures, on vehicular communication system using reconfigurable intelligent surfaces (RIS) with Doppler mitigation. A closed-form expression for the received signal-to-noise-and-distortion ratio (SNDR) of an RIS-aided vehicular communication system with HWI is derived, and we also show that the average Doppler spread can be removed completely. The simulation results validate that RIS with HWI is able to bring promising average SNDR gain (e.g, 3.16 dB) of the received signal, while eliminating the average Doppler spread, and keeping the delay spread at a very low range. As a result, using the predictable positions of the vehicle, the phase shift set of RIS can be designed in advance, such that channel estimation is not necessary, resulting in lower implementation complexity.**

***Index Terms*—reconfigurable intelligent surfaces, Doppler effect, delay spread, hardware impairments, high-mobility vehicular communication**

I. Introduction

The vehicle with high mobility, e.g., high-speed train, has severe Doppler effect, resulting in superimposed fast fading channel between the transmitter and the receiver [1]. Furthermore, this issue brings about many design challenges such as channel modeling, Doppler shift compensation, time-varying channel estimation, beamforming design, and resource management to high-mobility vehicular communications nowadays [2]. Therefore, compensating technologies such as massive multiple-input and multiple-output (mMIMO) and millimeter wave (mmWave) have been already applied to the fifth-generation cellular system [3]. However, in the sixth-generation cellular system, these technologies may not perform very well since both mMIMO and mmWave have disadvantages on high hardware costs, energy consumptions and computational complexities. Given this background, RIS has emerged as a promising technology to leverage these challenges [4], [5].

Recently, RIS has attracted widespread attention in vehicular communication to enhance the quality of transmission, due to its ability to control the complicated propagation environment [6], [7]. In [8], the authors revisit the multipath fading phenomenon in the context of RIS, and they show that using real-time tunable RIS, the rapid fluctuations caused by the Doppler effect in received signal strength can be effectively reduced. Besides, [9] proposes a novel and efficient channel estimation scheme by adding an RIS on a high-speed moving vehicle to assist the communication between its passenger and a static base station (BS). However, [6]–[9] all need channel estimation, which can be difficult to realize especially in the mobile scenario with high-speed vehicles. The authors in [10] propose to use useful information such as location and mobility pattern to design an RIS phase shift set in advance, which helps to reduce the complexity for beamforming, but the validation scenario considered is low-Earth orbit instead of the high-speed vehicular communication system. Inspired by [10], the authors in [11] introduce a novel anti-Doppler spread technique in high-mobility vehicular communication with RIS.

The works [6]–[11] are all based on the assumption of perfect RIS hardware. However, in most practical situations, inherent hardware impairments, e.g., phase noises, quantization errors, random failures, which generally limit the system performance, must be considered because of the non-idealities of the communication devices in the real world [12]–[14]. The authors in [13] investigate the rate performance of RIS-aided networks with HWI and then compare it theoretically to relay-aided networks. Considering three cases of the channel state information availability, the authors in [14] develop diagnostic techniques for RIS systems to identify and locate faulty reflecting elements and retrieve failure parameters. To the best of the authors' knowledge, there is no paper in the technical literature that examines the impact of hardware imperfections on the Doppler and delay spread of RIS-aided vehicular communication. In this paper, we

- present a general model to accommodate the impact of hardware imperfections on Doppler and delay spread of RIS-aided vehicular communication.
- obtain a suboptimal solution for a multi-objective problem, which aims to maximize SNDR, remove Doppler spread, and keep delay spread at a low level. Since the trajectory of the vehicle is predictable, channel estimation is not needed.
- reveal that in an RIS-aided vehicular communication system with HWI, the average Doppler and delay spread could be eliminated completely and be kept at a very low range, respectively.
- numerically validate the effectiveness and robustness of the RIS-aided vehicular communication system with HWI.

978-1-6654-2390-8/21/$31.00 ©2021 IEEE
Authorized licensed use limited to: Macao Polytechnic University. Downloaded on July 24,2026 at 07:02:40 UTC from IEEE Xplore. Restrictions apply.

Notation: Lower-case boldface letters denote the column vector. Upper-case calligraphic letters symbolize the phase shift set. U is continuous uniform distribution. The functions $(x \bmod y)$, $\lceil \cdot \rceil$ and $\lfloor \cdot \rfloor$ refer to the remainder of the division of x by y, the ceiling, and the floor of the argument, respectively. Further, the set of integer is denoted by $\mathbb{Z}$, $|\cdot|$ is the absolute value, and $\|\cdot\|$ represents the l_2 norm.

II. System Model

We consider a downlink RIS-aided high-mobility vehicular communication system, where both of the fixed BS and moving vehicle are equipped with a single isotropic antenna. As shown in Fig. 1, the RIS is a uniform planar array (UPA) composed of $M \times N$ elements which are placed on a rectangular grid spaced a and b apart in the $x-y$ plane in the three-dimensional (3D) Cartesian coordinate system, and the height of the RIS is h. Moreover, we assume that the vehicle moves at a high constant speed of v meters/second (m/s), the trajectory of the vehicle is along with the positive direction of the x-axis, and the position of the vehicle is assumed to be known, given the speed v, the direction, and the schedule information.

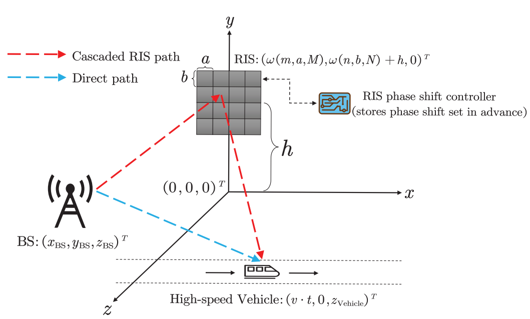

Fig. 1. An RIS-aided high-mobility vehicle communication system.

A. Geometry of the RIS

As shown in Fig. 1, assume that the geometric center of the RIS in the 3D Cartesian coordinate system is $(0, h, 0)^T$, the coordinate of the (m, n)th element of the RIS can be calculated as [10]

$$\boldsymbol{p}_{m,n} = \Big(\omega(m,a,M), \omega(n,b,N) + h, 0\Big)^T, \tag{1}$$

where $\omega(m,a,M) = a[m-0.5((M+1) \bmod 2)]$, $m \in \Omega(M)$, $n \in \Omega(N)$ and

$$\Omega(M) = \left\{[(M+1) \bmod 2)] - \left\lfloor \frac{M}{2} \right\rfloor, \ldots, \left\lfloor \frac{M}{2} \right\rfloor\right\}. \tag{2}$$

Note that $\omega(n,b,N)$ and $\Omega(N)$ are obtained in the same way as $\omega(m,a,M)$ and $\Omega(M)$, respectively.

B. Amplitude Gains and Time Delays for Direct Path

We first consider the direct path and the cascaded RIS path are all line-of-sight (LOS) without hardware impairment. If the transmitter locates at $\boldsymbol{p}_{\mathrm{T}}$ and the instantaneous time is t, then the direct path amplitude gain A_0 is

$$A_0 = \frac{\lambda_c \sqrt{G_{\mathrm{T}}^{\mathrm{R}}(t) G_{\mathrm{R}}^{\mathrm{T}}(t)}}{4\pi \|\boldsymbol{p}_{\mathrm{R}}(t) - \boldsymbol{p}_{\mathrm{T}}\|}, \tag{3}$$

where $G_{\mathrm{T}}^{\mathrm{R}}(t)$ is the instantaneous transmitter antenna gain when the observation point is the receiver antenna, and $G_{\mathrm{R}}^{\mathrm{T}}(t)$ is the instantaneous receiver antenna gain when the observation point is transmitter antenna. λ_c denotes the wavelength of the signal, and $\|\boldsymbol{p}_{\mathrm{R}}(t) - \boldsymbol{p}_{\mathrm{T}}\|$ is the Euclidean distance between the transmitter and the receiver at time t.

Accordingly, for the direct path, the baseband signal received by the receiver antenna at time t is

$$S_0(t) = A_0 \left[\sqrt{P_T} x\Big(t - \tau_0(t)\Big)\right], \tag{4}$$

where $x(t)$ is the transmitted signal with unit power, P_{T} denotes the transmit power, and $\tau_0(t)$ is the time delay from the transmitter to the receiver in the direct path, given as

$$\tau_0(t) = \frac{\|\boldsymbol{p}_{\mathrm{R}}(t) - \boldsymbol{p}_{\mathrm{T}}\|}{c}, \tag{5}$$

where c is the speed of light.

C. Amplitude Gains and Time Delays for Cascaded RIS Path

Based on (3) and (5), and assume $G_{\mathrm{T}}^{m,n} = G_{\mathrm{R}}^{m,n}(t) = 1$, we then obtain the amplitude gain $A_{m,n}$ and time delay $\tau_{m,n}(t)$ for the cascaded RIS path as

$$A_{m,n} = \frac{\lambda_c^2 \sqrt{G_{m,n}^{\mathrm{T}} G_{m,n}^{\mathrm{R}}(t)}}{16\pi^2 \|\boldsymbol{p}_{m,n} - \boldsymbol{p}_{\mathrm{T}}\| \|\boldsymbol{p}_{\mathrm{R}}(t) - \boldsymbol{p}_{m,n}\|}, \tag{6}$$

$$\tau_{m,n}(t) = \frac{\|\boldsymbol{p}_{m,n} - \boldsymbol{p}_{\mathrm{T}}\|}{c} + \frac{\|\boldsymbol{p}_{\mathrm{R}}(t) - \boldsymbol{p}_{m,n}\|}{c}. \tag{7}$$

Note that $G_{m,n}^{\mathrm{T}} = \frac{4\pi}{\lambda_c^2} ab\cos(\theta_T)$ and $G_{m,n}^{\mathrm{R}}(t) = \frac{4\pi}{\lambda_c^2} ab\cos(\theta_R(t))$, where $\theta_T = \arccos(\frac{z_{m,n} - z_{\mathrm{T}}}{\|\boldsymbol{p}_{m,n} - \boldsymbol{p}_{\mathrm{T}}\|})$ and $\theta_R(t) = \arccos(\frac{z_{m,n} - z_{\mathrm{R}}}{\|\boldsymbol{p}_{m,n} - \boldsymbol{p}_{\mathrm{R}}(t)\|})$. As such, for the m,n-th element in the cascaded RIS path, the baseband signal at time t is

$$S_{m,n}(t) = A_{m,n}(t) \left[\sqrt{P_T} x\left(t - \tau_{m,n}(t) - \frac{\phi_{m,n}(t)}{2\pi f_c}\right)\right], \tag{8}$$

where $\phi_{m,n}(t)$ is phase shift by the m,n-th element of RIS. Finally, the baseband complex received signal can be written as

$$\begin{aligned} y(t) =& S_0(t) e^{-j2\pi f_c \tau_0(t)} \\ &+ \sum_{m,n} S_{m,n}(t) e^{-j2\pi f_c \tau_{m,n}(t) - j\phi_{m,n}(t)} + n(t), \end{aligned} \tag{9}$$

where $n(t) \sim \mathcal{CN}(0, \sigma^2)$ denotes the receiver noise.

Authorized licensed use limited to: Macao Polytechnic University. Downloaded on July 24,2026 at 07:02:40 UTC from IEEE Xplore. Restrictions apply.

III. Doppler Mitigation without Hardware Impairments

Using (9), *the instantaneous signal-to-noise ratio* (SNR) of the received signal $y(t)$ can be calculated as

$$\mathrm{SNR}(t) = \frac{P_R(t)}{\sigma^2}, \tag{10}$$

where $P_R(t)$ represents the received signal power.

At time t, the Doppler spread between the direct path and the cascaded path is

$$D_{s,0}(t) = f_c \max_{m,n} \left| \frac{d}{dt}\left(\tau_{m,n}(t) + \frac{\phi_{m,n}(t)}{2\pi f_c}\right) - \frac{d}{dt}\tau_0(t)\right|. \tag{11}$$

Similarly, the Doppler spread of the RIS itself at time t is

$$\begin{aligned} D_{s,\mathrm{RIS}}(t) = f_c \max_{m,n,m',n'} \Bigg| \frac{d}{dt}\left(\tau_{m,n}(t) + \frac{\phi_{m,n}(t)}{2\pi f_c}\right) \\ - \frac{d}{dt}\left(\tau_{m',n'}(t) + \frac{\phi_{m',n'}(t)}{2\pi f_c}\right)\Bigg|. \end{aligned} \tag{12}$$

Since *Doppler spread* is the largest frequency difference over the direct and cascaded paths [10], we have *the instantaneous Doppler spread* over all paths as

$$D_s(t) = \max\{D_{s,0}(t), D_{s,\mathrm{RIS}}(t)\}. \tag{13}$$

The delay spread between the direct path and the cascaded path at time t is

$$T_{d,0}(t) = \max_{m,n}\left\{\tau_{m,n}(t) + \frac{\phi_{m,n}(t)}{2\pi f_c}\right\} - \tau_0(t), \tag{14}$$

and the delay spread across the RIS at time t is

$$\begin{aligned} T_{d,\mathrm{RIS}}(t) = &\max_{m,n}\left\{\tau_{m,n}(t) + \frac{\phi_{m,n}(t)}{2\pi f_c}\right\} \\ &- \min_{m,n}\left\{\tau_{m,n}(t) + \frac{\phi_{m,n}(t)}{2\pi f_c}\right\}. \end{aligned} \tag{15}$$

Since *delay spread* is defined as the largest time difference over the two paths, *the instantaneous delay spread* over all paths is

$$T_d(t) = \max\{T_{d,0}(t),\ T_{d,\mathrm{RIS}}(t)\}. \tag{16}$$

Aiming at maximizing $\mathrm{SNR}(t)$ at the receiver, while minimizing Doppler spread $D_s(t)$ and keeping delay spread $T_d(t)$ at a low range, we want to find a *Pareto optimal solution* for a multi-objective problem as follow [11]

$$\max_{\forall m,n:\phi_{m,n}(t)} \big[\mathrm{SNR}(t) \quad -D_{\mathrm{s}}(t) \quad -T_{\mathrm{d}}(t)\big]. \tag{17}$$

The most important objective of (17) is to maximize the instantaneous SNR at time t. Minimizing Doppler and delay spread are the second and third objectives, respectively. Based on [11], the Pareto suboptimal solution can be found as

$$\mathcal{T}(t) = 2\pi\left[\big(f_c(\tau_0(t) - \tau_{m,n}(t))\big) \bmod 1\right]. \tag{18}$$

IV. Doppler Migration with Hardware Impairments

A. RIS and Transceiver Hardware Impairments

Since the non-ideality of the hardware cannot be avoided, the received signal is disturbed by the HWI which exists in practical devices [12]. At first, we would derive the expression of the received signal with *the RIS hardware impairments* (RIS-HWI). For the system model described in (9), the RIS-HWI can be regarded as random phase errors in RIS, which decreases the system performance [15]. Assuming that the random phase error exists in the m,n-th element of RIS at time t, (8) can be modified to include RIS-HWI as

$$\begin{aligned} &S^{\mathrm{R}}_{m,n}(t) = A_{m,n}(t) \\ &\left[\sqrt{P_T}x\left(t - \tau_{m,n}(t) - \frac{\phi_{m,n}(t) - \rho_{m,n}(t)}{2\pi f_c}\right)\right], \end{aligned} \tag{19}$$

where $\rho_{m,n}(t)$ is stationary process with the following probability density function (PDF)

$$f_\rho(x,t) = \begin{cases} \frac{1}{b_\rho - a_\rho} & ,\ a_\rho \le x \le b_\rho \\ 0 & ,\ x < a_\rho \text{ or } x > b_\rho. \end{cases} \tag{20}$$

Secondly, *the transceiver hardware impairments* (T-HWI) can be modeled as additive distortion noises both in transmitter and receiver [13]. More precisely, assume $\eta_T(t)$ and $\eta_R(t)$ are stationary complex Gaussian processes for the distortion noises generated by the transmitter and receiver, respectively, then we can rewrite (4) and (19) as

$$S^{\mathrm{T}}_0(t) = A_0\left[\sqrt{P_T}x\Big(t - \tau_0(t)\Big) + \eta_T(t)\right], \tag{21}$$

and

$$\begin{aligned} &S^{\mathrm{RT}}_{m,n}(t) = A_{m,n}(t)\Bigg[\sqrt{P_T} \\ &x\left(t - \tau_{m,n}(t) - \frac{\phi_{m,n}(t) - \rho_{m,n}(t)}{2\pi f_c}\right) + \eta_T(t)\Bigg]. \end{aligned} \tag{22}$$

Hence, (9) can be modified to include RIS-HWI and T-HWI as

$$\begin{aligned} &y^{\mathrm{RT}}(t) = S^{\mathrm{T}}_0(t)e^{-j2\pi f_c\tau_0(t)} + \sum_{m,n} S^{\mathrm{RT}}_{m,n}(t) \\ &e^{-j2\pi f_c\tau_{m,n}(t) - j\phi_{m,n}(t) + j\rho_{m,n}(t)} + \eta_R(t) + n(t), \end{aligned} \tag{23}$$

where the power spectral density of $\eta_T(t)$ and $\eta_R(t)$ are $\kappa_t P_T$ and $\kappa_r|y(t) - n(t)|^2$, respectively. κ_t is the transmitter's error vector magnitude (EVM) and κ_r is the EVM of the receiver. The typical value of κ_t and κ_r are the same, ranging from 0.01^2 to 0.15^2 [12].

Authorized licensed use limited to: Macao Polytechnic University. Downloaded on July 24,2026 at 07:02:40 UTC from IEEE Xplore. Restrictions apply.

B. Random Failures for the Elements

Faulty reflecting elements of RIS can be denoted by the *failure mask* function $\Gamma_{m,n}$ [14]. Assume this function is time-invariance for one vehicle pass, then we have

$$\Gamma_{m,n}=\begin{cases}1 & \text{if the } m,n\text{-th element is functioning}\\ \zeta_{m,n}e^{j\delta_{m,n}} & \text{if the } m,n\text{-th element is faulty}\end{cases} \tag{24}$$

where $\zeta_{m,n}\sim U[0,1]$ and $\delta_{m,n}\sim U[0,2\pi]$. Then, $y^{\mathrm{RT}}(t)$ with random failure (RFA) can be expressed as follow

$$y^{\mathrm{RTF}}(t)=S_0^{\mathrm{T}}(t)e^{-j2\pi f_c\tau_0(t)}+\sum_{m,n}\Gamma_{m,n}S_{m,n}^{\mathrm{RT}}(t)\\ e^{-j2\pi f_c\tau_{m,n}(t)-j\phi_{m,n}(t)+j\rho_{m,n}(t)}+\eta_R(t)+n(t). \tag{25}$$

C. Phase Quantization Errors of RIS

When only a discrete set of 2^q phases can be configured, $q\geq 1$, the phase quantization error (PQE) of RIS is assumed to be uniformly distributed over $[-2^{-q}\pi, 2^{-q}\pi]$ [15]. In this paper, we assume that the PQE $\gamma_{m,n}(t)$ is a stationary process with uniform distribution for one vehicle pass. The PDF of $\gamma_{m,n}(t)$ is

$$f_\gamma(x,t)=\begin{cases}\frac{1}{b_\gamma-a_\gamma} & ,\ a_\gamma\leq x\leq b_\gamma\\ 0 & ,\ x<a_\gamma \text{ or } x>b_\gamma.\end{cases} \tag{26}$$

Then, using (23) and (25), we can obtain a general model to accommodate the impact of HWI for Doppler and delay spread as

$$y^{\mathrm{HWI}}(t)=S_0^{\mathrm{T}}(t)e^{-j2\pi f_c\tau_0(t)}+\sum_{m,n}\Gamma_{m,n}S_{m,n}^{\mathrm{RTP}}(t)\\ e^{-j2\pi f_c\tau_{m,n}(t)-j\phi_{m,n}(t)+j\rho_{m,n}(t)+j\gamma_{m,n}(t)}+\eta_R(t)+n(t) \tag{27}$$

with

$$S_{m,n}^{\mathrm{RTP}}(t)=A_{m,n}(t)\Bigg[\sqrt{P_T}x\bigg(t-\tau_{m,n}(t)\\ -\frac{\phi_{m,n}(t)-\rho_{m,n}(t)-\gamma_{m,n}(t)}{2\pi f_c}\bigg)+\eta_T(t)\Bigg]. \tag{28}$$

Therefore, based on (21) and (27), we obtain the SNDR for $y^{\mathrm{HWI}}(t)$ as

$$\mathrm{SNDR}(t)=\frac{|\Upsilon(t)+\Lambda(t)|^2}{\kappa_t|\Upsilon(t)+\Lambda(t)|^2+\kappa_r|\Upsilon(t)+\Lambda(t)|^2+\sigma^2}. \tag{29}$$

where

$$\Upsilon(t)\triangleq\bigg[S_0^{\mathrm{T}}(t)-A_0\eta_T(t)\bigg]e^{-j2\pi f_c\tau_0(t)},$$

and

$$\Lambda(t)\triangleq\sum_{m,n}\Gamma_{m,n}\bigg[S_{m,n}^{\mathrm{RTP}}(t)-A_{m,n}(t)\eta_T(t)\bigg]\\ e^{-j2\pi f_c\tau_{m,n}(t)-j\phi_{m,n}(t)+j\rho_{m,n}(t)+j\gamma_{m,n}(t)}.$$

D. Mitigating Doppler Effects for RIS with Hardware Impairments

Based on (11)-(13), (27), and ignore RFA for simplicity, the Doppler spread between the direct path and the RIS with RIS-HWI, T-HWI and PQE can be calculated as

$$D_{s,0}^{\mathrm{HWI}}(t)=f_c\max_{m,n}\Bigg|\frac{d}{dt}\bigg(\tau_{m,n}(t)\\ +\frac{\phi_{m,n}(t)-\rho_{m,n}(t)-\gamma_{m,n}(t)}{2\pi f_c}\bigg)-\frac{d}{dt}\tau_0(t)\Bigg|. \tag{30}$$

Then, substituting (18) into (30), we obtain

$$D_{s,0}^{\mathrm{HWI}}(t)=f_c\max_{m,n}\Bigg|\frac{d}{dt}\bigg(\rho_{m,n}(t)+\gamma_{m,n}(t)\bigg)\Bigg|, \tag{31}$$

and based on (12), the Doppler spread of the RIS itself with HWI, $D_{s,\mathrm{RIS}}^{\mathrm{HWI}}(t)$, is obtained in the same way.

The study of Doppler effects requires to drop the time-invariance assumption [16]. Therefore, we have the expectation of $D_{s,0}^{\mathrm{HWI}}(t)$ as

$$\mathbb{E}\bigg\{D_{s,0}^{\mathrm{HWI}}(t)\bigg\}=\\ \mathbb{E}\Bigg\{f_c\max_{m,n}\Bigg|\frac{d}{dt}\bigg(\rho_{m,n}(t)\bigg)+\frac{d}{dt}\bigg(\gamma_{m,n}(t)\bigg)\Bigg|\Bigg\}. \tag{32}$$

Since stationary process $\rho_{m,n}(t)$ satisfies the condition of the differentiability, we have

$$\mathbb{E}\bigg\{\frac{d}{dt}[\rho_{m,n}(t)]\bigg\}=\frac{d}{dt}\bigg[\mathbb{E}\bigg\{\rho_{m,n}(t)\bigg\}\bigg]. \tag{33}$$

Based on (21), and due to the stationary property of $\rho_{m,n}(t)$, we have

$$\frac{d}{dt}\bigg[\mathbb{E}\bigg\{\rho_{m,n}(t)\bigg\}\bigg]=\frac{d}{dt}\bigg[\int_{a_\rho}^{b_\rho}xf_\rho(x,t)dx\bigg]=0. \tag{34}$$

Similarly, $\frac{d}{dt}\bigg[\mathbb{E}\bigg\{\gamma_{m,n}(t)\bigg\}\bigg]=0$, then $\mathbb{E}\bigg\{D_{s,0}^{\mathrm{HWI}}(t)\bigg\}=0$. It is also not hard to show $\mathbb{E}\bigg\{D_{s,\mathrm{RIS}}^{\mathrm{HWI}}(t)\bigg\}=0$ and $\mathbb{E}\bigg\{D_{s}^{\mathrm{HWI}}(t)\bigg\}=0$. Therefore, although the HWI brings extra instantaneous Doppler spread, the average Doppler spread for one vehicle pass is still zero.

Also, based on (14), (15), their corresponding delay spread with HWI can be written as

$$T_{d,0}^{\mathrm{HWI}}(t)=\max_{m,n}\bigg\{\tau_{m,n}(t)+\frac{\phi_{m,n}(t)-\rho_{m,n}(t)-\gamma_{m,n}(t)}{2\pi f_c}\bigg\}\\ -\tau_0(t), \tag{35}$$

Authorized licensed use limited to: Macao Polytechnic University. Downloaded on July 24,2026 at 07:02:40 UTC from IEEE Xplore. Restrictions apply.

$$T_{d,\text{RIS}}^{\text{HWI}}(t) = \max_{m,n}\left\{\tau_{m,n}(t) + \frac{\phi_{m,n}(t) - \rho_{m,n}(t) - \gamma_{m,n}(t)}{2\pi f_c}\right\} - \min_{m,n}\left\{\tau_{m,n}(t) + \frac{\phi_{m,n}(t) - \rho_{m,n}(t) - \gamma_{m,n}(t)}{2\pi f_c}\right\}. \tag{36}$$

Finally, the maximum delay spread with HWI can be calculated as

$$\begin{aligned} T_d^{\text{HWI}}(t) &= \max\{T_{d,0}\text{HWI}(t),\ T_{d,\text{RIS}}\text{HWI}(t)\} \\ &= T_{d,0}^{\text{HWI}}(t). \end{aligned} \tag{37}$$

From (37), we can see that the delay spread $T_d^{\text{HWI}}(t)$ is affected by the HWI. However, since f_c is usually very large, compared to $\phi_{m,n}(t)$, $\rho_{m,n}(t)$, and $\gamma_{m,n}(t)$, the total delay spread $T_d^{\text{HWI}}(t)$ still can be kept at a relatively low range. From Fig. 2, assume all three cases with the same 2-bit quantization but different RIS-HWIs, it can be seen that all kinds of $T_d^{\text{HWI}}(t)$ are kept to very small values in a typical high-speed vehicle communication scenario. It is worth noting that the delay spread (with and without HWI) decreases when the vehicle approaches the BS. This is because τ_0 and τ_{mn} are determined by $\|\boldsymbol{p}_{\text{R}}(t)-\boldsymbol{p}_{\text{T}}\|$ and $\|\boldsymbol{p}_{\text{R}}(t)-\boldsymbol{p}_{m,n}\|$, respectively. However, when the vehicle is far from the BS (e.g., after $t = 55$ s), the delay spread would be almost static.

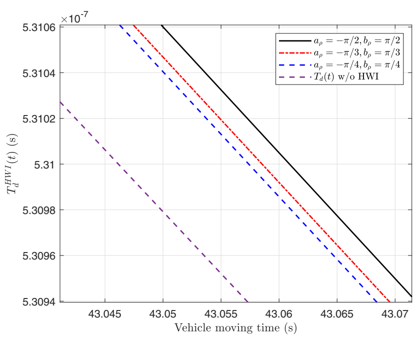

Fig. 2. $T_d^{\text{HWI}}(t)$ for one vehicle pass. All the cases with 2-bit quantization and different RIS-HWIs .

V. Simulation Results

In this section, numerical examples are provided to validate the robustness and the effectiveness of the suboptimal solution phase set $\mathcal{T}(t)$ under HWI. We consider a 3D Cartesian coordinate system where a single RIS locates on $x-y$ plane, $M = N = 256$ and $a = b = \frac{\lambda}{5}$. The height of the RIS is $h = 20$ m, the vehicle moves at a speed of $v = 83.3$ m/s, and the trajectory of the vehicle is straight along the positive x-axis direction. Moreover, the BS is located at (-50 m, 100 m, 50 m), the vehicle is located at ($v \cdot t$ m, 0 m, 100 m) where $t \in \mathbb{Z}$ and its range is from 1 s to 100 s. The start point of the vehicle is (-4000 m, 0 m, 100 m), the carrier frequency is 2.4 GHz. Besides, the transmit power P_T is set to 20 dBm and σ^2 is -80 dBm. We also assume unobstructed view, no atmospheric effects, and all paths are LOS.

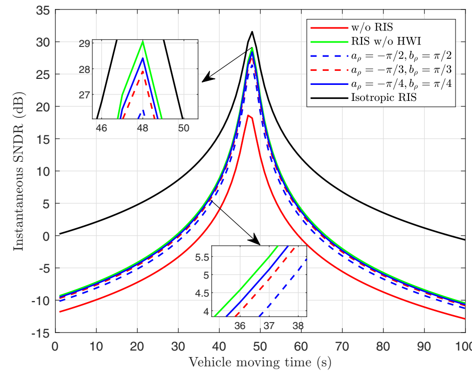

Fig. 3. Instantaneous SNDR for one vehicle pass. The RIS is only with different RIS-HWIs.

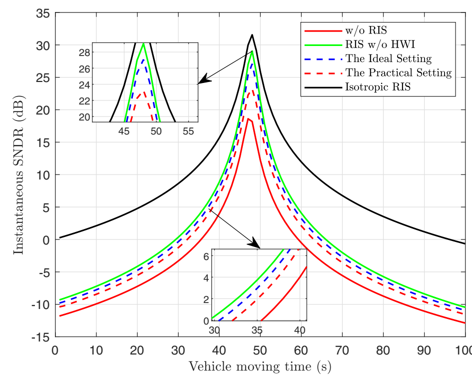

Fig. 4. Instantaneous SNDR for one vehicle pass. The RIS is with the ideal and practical setting, respectively.

Three benchmarks are used, i.e., 1) without RIS, 2) HWI-free isotropic RIS (i.e., $G_{m,n}^{\text{T}} = G_{m,n}^{\text{R}}(t) = 1$) with phase shift set $\mathcal{T}(t)$ and 3) HWI-free RIS with phase shift set $\mathcal{T}(t)$. The isotropic RIS is used as an upper bound that serves as an optimal case, and the lower bound is the transmission without RIS.

Fig. 3 shows the performances for RIS only with RIS-HWI. It can be seen that the $a_\rho = -\pi/2, b_\rho = \pi/2$ case performs the worst, as expected. However, even in this unsatisfied case, the SNDR gain still can be achieved from 1.62 dB to 8.25 dB for one vehicle pass. Besides, at time $t = 48$ s, the performances of all kinds of RISs are the best since in (6), the minimum value of $\|\boldsymbol{p}_{\text{R}}(t) - \boldsymbol{p}_{m,n}\|$ is achieved at this time, i.e., the largest amplitude gain $A_{m,n}$ is obtained. Similarly, we can also observe the same pattern for the SNDR gain performance for different T-HWIs, PQEs and RFAs.

In Table A, we summarize and compare the SNDR gain for one vehicle pass (i.e., from $t = 1$ s to $t = 100$ s) with different HWIs. The minimum, average and maximum value of SNR gain for different cases are investigated. For RIS-HWI,

Authorized licensed use limited to: Macao Polytechnic University. Downloaded on July 24,2026 at 07:02:40 UTC from IEEE Xplore. Restrictions apply.

TABLE A
SNDR GAIN COMPARISON WITH DIFFERENT HWIS.

Different HWIs / SNDR gain (dB)	without HWI	RIS-HWI ($\pi/4, \pi/3, \pi/2$)	T-HWI ($0.01^2, 0.03^2, 0.05^2$)	PQE (3-bit, 2-bit, 1-bit)
Minimum	2.43	2.21, 2.05, 1.62	2.43, 2.43, 2.43	2.37, 2.21, 1.62
Average	3.89	3.58, 3.35, 2.70	3.87, 3.75, 3.59	3.81, 3.58, 2.70
Maximum	10.87	10.23, 9.72, 8.25	10.35, 8.40, 6.90	10.71, 10.23, 8.25
Different HWIs / SNDR gain (dB)	without HWI	RFA (1%, 3%, 5%)	Ideal Setting	Practical Setting
Minimum	2.43	2.40, 2.36, 2.32	1.94	1.32
Average	3.89	3.86, 3.80, 3.73	3.16	2.16
Maximum	10.87	10.81, 10.68, 10.55	8.95	5.87

we assume 1) $a_\rho = -\frac{\pi}{4}$, $b_\rho = \frac{\pi}{4}$, 2) $a_\rho = -\frac{\pi}{3}$, $b_\rho = \frac{\pi}{3}$ and 3) $a_\rho = -\frac{\pi}{2}$, $b_\rho = \frac{\pi}{2}$. For T-HWI, 1) $\kappa_t = \kappa_r = 0.01^2$, 2) $\kappa_t = \kappa_r = 0.03^2$ and 3) $\kappa_t = \kappa_r = 0.05^2$ are considered. For PQE and RFA, we assume 1) 3-bit, 2) 2-bit and 3) 1-bit quantization, and 1) 1%, 2) 3% and 3) 5% failure rate [14], respectively. The ideal and practical setting cases are also included in this table. It is interesting to note that when the SNDR decreases, different T-HWI cases have almost the same SNDR gain. In other words, T-HWI is not the dominant factor that degrades the performance of the whole RIS system when the SNDR is low.

Fig. 4 depicts the ideal and practical setting performances for one vehicle pass. For the ideal setting, we use 3-bit quantization since it is good enough to mimic the continuous phase set [17]. The elements of the RIS are in good condition so $a_\rho = -\pi/4, b_\rho = \pi/4$. Besides, assume transceiver works well, then $\kappa_t = \kappa_r = 0.01^2$ [12], and the random failure rate is the smallest, i.e., 1%. For the practical setting, 2-bit quantization, $a_\rho = -\pi/3, b_\rho = \pi/3$, $\kappa_t = \kappa_r = 0.03^2$, and 3% random failure rate are used. The result shows that for the ideal setting scenario, the SNDR gain is from 1.94 dB to 8.95 dB. Moreover, we still have 2.16 dB average SNDR gain in the practical setting scenario for one vehicle pass.

VI. Conclusions

In this work, we have analyzed the effects of different hardware impairments on an RIS-aided Doppler effect mitigating vehicular communication system. The SNDR expression of the received signal with HWI is obtained, and we show that the average Doppler and delay spread can be eliminated and be kept at a low range, respectively. The simulation results validate the robustness and effectiveness of the RIS with HWI in the mobile scenario with high-speed vehicles. Although the HWI cannot be avoided, the RIS still can provide 3.16 dB average SNDR gain. Doppler mitigation using multiple RISs with HWI is left open for future work.

References

[1] D. Tse and P. Viswanath, *Fundamentals of Wireless Communication*. Cambridge university press, 2005.

[2] H. Liu, J. Zhang, Q. Wu, Y. Jin, Y. Chen, and B. Ai, "RIS-Aided Next-Generation High-Speed Train Communications: Challenges, Solutions, and Future Directions," *arXiv preprint arXiv:2103.09484*, 2021.

[3] B. Ai, A. F. Molisch, M. Rupp, and Z.-D. Zhong, "5G Key Technologies for Smart Railways," *Proceedings of the IEEE*, vol. 108, no. 6, pp. 856–893, 2020.

[4] Q. Wu and R. Zhang, "Towards Smart and Reconfigurable Environment: Intelligent Reflecting Surface Aided Wireless Network," *IEEE Communications Magazine*, vol. 58, no. 1, pp. 106–112, 2020.

[5] M. Renzo, A. Zappone, M. Debbah, M. S. Alouini, and S. Tretyakov, "Smart Radio Environments Empowered by Reconfigurable Intelligent Surfaces: How it Works, State of Research, and Road Ahead," *IEEE Journal on Selected Areas in Communications*, vol. 38, no. 11, pp. 2450–2525, 2020.

[6] A. U. Makarfi, K. M. Rabie, O. Kaiwartya, X. Li, and R. Kharel, "Physical Layer Security in Vehicular Networks with Reconfigurable Intelligent Surfaces," in *2020 IEEE 91st Vehicular Technology Conference (VTC2020-Spring)*. IEEE, 2020, pp. 1–6.

[7] Y. Chen, Y. Wang, J. Zhang, and Z. Li, "Resource Allocation for Intelligent Reflecting Surface Aided Vehicular Communications," *IEEE Transactions on Vehicular Technology*, vol. 69, no. 10, pp. 12 321–12 326, 2020.

[8] E. Basar, "Reconfigurable intelligent surfaces for doppler effect and multipath fading mitigation," *Frontiers in Communications and Networks*, vol. 2, p. 14, 2021.

[9] Z. Huang, B. Zheng, and R. Zhang, "Transforming Fading Channel from Fast to Slow: IRS-Assisted High-Mobility Communication," in *ICC 2021-IEEE International Conference on Communications*. IEEE, 2021, pp. 1–6.

[10] B. Matthiesen, E. Björnson, E. De Carvalho, and P. Popovski, "Intelligent Reflecting Surface Operation under Predictable Receiver Mobility: A Continuous Time Propagation Model," *IEEE Wireless Communications Letters*, vol. 10, no. 2, pp. 216–220, 2021.

[11] K. Wang, C.-T. Lam, and B. K. Ng, "IRS-Aided Predictable High-Mobility Vehicular Communication with Doppler Effect Mitigation," in *2021 IEEE 93rd Vehicular Technology Conference (VTC2021-Spring)*. IEEE, 2021, pp. 1–6.

[12] E. Björnson, J. Hoydis, M. Kountouris, and M. Debbah, "Massive MIMO Systems with Non-ideal Hardware: Energy Efficiency, Estimation, and Capacity Limits," *IEEE Transactions on information theory*, vol. 60, no. 11, pp. 7112–7139, 2014.

[13] Z. Xing, R. Wang, J. Wu, and E. Liu, "Achievable rate analysis and phase shift optimization on intelligent reflecting surface with hardware impairments," *IEEE Transactions on Wireless Communications*, 2021.

[14] R. Sun, W. Wang, L. Chen, G. Wei, and W. Zhang, "Diagnosis of Intelligent Reflecting Surface in Millimeter-wave Communication Systems," *arXiv preprint arXiv:2101.03792*, 2021.

[15] M. Badiu and J. P. Coon, "Communication through a Large Reflecting Surface with Phase Errors," *IEEE Wireless Communications Letters*, vol. 9, no. 2, pp. 184–188, 2020.

[16] E. Björnson, H. Wymeersch, B. Matthiesen, P. Popovski, L. Sanguinetti, and E. de Carvalho, "Reconfigurable Intelligent Surfaces: A Signal Processing Perspective with Wireless Applications," *arXiv preprint arXiv:2102.00742*, 2021.

[17] Q. Wu and R. Zhang, "Beamforming Optimization for Intelligent Reflecting Surface with Discrete Phase Shifts," in *2019 IEEE International Conference on Acoustics, Speech and Signal Processing (ICASSP)*, 2019, pp. 7830–7833.

Authorized licensed use limited to: Macao Polytechnic University. Downloaded on July 24,2026 at 07:02:40 UTC from IEEE Xplore. Restrictions apply.